Iranian Journal of Medical Physics

ijmp.mums.ac.ir

Telecobalt Machine Beam Intensity Modulation with Aluminium Compensating Filter Using Missing Tissue Approach

Samuel Nii Adu Tagoe[1*] , Samuel Yeboah Mensah[2] , John Justice Fletcher[3] , Evans Sasu[4] ,

1. Department of Physics, School of Applied Physical Sciences, University of Cape Cost, Cape Coast, Ghana, National Centre for Radiotherapy and Nuclear Medicine, Korle Bu Teaching Hospital, Accra, Ghana
2. Department of Physics, School of Applied Physical Sciences, University of Cape Cost, Cape Coast, Ghana.
3. Department of Applied Physics, University for Development Studies, Navrongo Campus, Navrongo, Ghana
4. National Centre for Radiotherapy and Nuclear Medicine, Korle Bu Teaching Hospital, Accra, Ghana.

ARTICLE INFO

Article type:
Original Article

Article history:
Received: Jul 25, 2017
Accepted: Aug 31, 2017

Keywords:
Compensating Filter
Bolus
Regression
Modulation

ABSTRACT

Introduction: The present study aimed to generate intensity-modulated beams with Aluminium compensating filters for a conventional telecobalt machine based on the outputs of a treatment planning system (TPS) performing forward planning and cannot simulate directly the compensating filter.

Materials and Methods: In order to achieve the beam intensity modulation during treatment planning with the TPS, we used a bolus placed on the surface of a tissue-equivalent phantom. The treatment plans replicated on the telecobalt machine with the bolus were represented with compensating filters placed at a certain distance from the phantom surface. An equation was proposed for the conversion of the bolus thickness to the compensating filter thickness such that any point within the phantom would receive the planned dose. Correction factors were introduced into the proposed equation to account for the influences of field size, treatment depth, and applied bolus thickness. The proposed equation was obtained based on the analyses of empirical data measured in a full scatter water phantom with and without the compensating filter.

Results: According to the results, the dosimetric verification of the proposed approach outputs in a solid water phantom with calibrated Gafchromic EBT2 films were comparable to that of the TPS with deviation of ±4.73% (mean: 2.98±1.05%).

Conclusion: As the findings of the present study indicated, the discrepancy between the measured doses and TPS-estimated doses was within the tolerance of ±5%, which is recommended for dose delivery in external beam radiotherapy. Therefore, the proposed approach is recommended for clinical application.

► *Please cite this article as:*
Tagoe S, Mensah S, Fletcher J, Sasu E. Telecobalt Machine Beam Intensity Modulation with Aluminium Compensating Filter Using Missing Tissue Approach. Iran J Med Phys 2018; 15: 48-61. 10.22038/ijmp.2017.23548.1253.

Introduction

Dose distribution within the irradiated region is the most reliable and verifiable quantity linking the treatment parameters to observed therapeutic outcomes for specific treatment technique in radiotherapy [1]. It is imperative to accurately know the dose that would be deposited at any point within the patient undergoing external beam radiotherapy (EBRT). It is also practically impossible to put radiation detectors within the patient subjected to irradiation.

The dose distributions within a patient are mostly calculated with the aid of dosimetric functions determined in a full scatter water phantom and mathematical algorithms that are aimed to explain the physics of the radiation interactions with a medium or matter [1, 2]. To enhance the efficiency of dose computation and speed up this process, specialized computers known as treatment planning systems (TPSs) are used to simulate the treatment process for the realization of therapeutic intent prior to treatment delivery.

The process of simulating the treatment delivery process with a computer is referred to as treatment planning. Nonetheless, this process goes beyond the sole treatment simulation and determines the dose distribution within the patient, which is usually associated with treatment duration. Treatment planning also involves all the steps needed for the effective management of a patient.

*Corresponding Author: Department of Physics, School of Applied Physical Sciences, University of Cape Cost, Cape Coast, Ghana, National Centre for Radiotherapy and Nuclear Medicine, Korle Bu Teaching Hospital, Accra, Ghana, Email: s.tagoe@kbth.gov.gh, Tel: +233244268061

These steps include patient diagnoses to help the clinicians stage the disease and select the optimal treatment modalities, imaging to facilitate the effective localization of the intended target and the surrounding normal tissues, radiation dose optimization to facilitate the selection of irradiation geometries maximizing doses to the intended target volume and minimizing doses to the normal tissues, as well as treatment plan evaluation to assess the adequacies of the chosen irradiation geometries.

Therefore, TPSs are used as radiation dose optimization tools for treatment delivery in EBRT. Forward and inverse plannings are two variants of treatment planning technique that can be performed in a TPS. Forward planning is assigned to a condition when the planner selects beams and provides their orientations as well as weightings. In this kind of planning, the TPS calculates the resultant dose distribution within the irradiated region based on the selected irradiation geometries.

On the other hand, in the -inverse planning, the planner selects the beams, provides their orientations, and indicates the desired dose distributions and constraints within the irradiated region. In this type, the TPS applies the necessary beam weightings and modulations that will give rise to the desired dose distributions within the patient. The lack of appropriate treatment equipment and/or paucity of resources affect the ability to optimize the radiation dose to an irradiated target.

During EBRT, the spatial distribution of radiation dose within a patient is influenced by a lot of factors, such as surface topography at the point of beam entrance and tissue inhomogeneities within the irradiated region [2]. These factors along with the complex shape of an irradiated target volume (tumor) call for the modulation of the beam fluence distribution across the individual radiation fields. This modulation facilitates the optimization of the radiation dose to the intended target volume while minimizing radiation dose to the neighboring normal tissues. This has been culminated in the introduction of intensity-modulated radiotherapy (IMRT).

The implementation of IMRT needs the fulfillment of basic requirements. One of these requirements is the availability of a TPS with inverse or forward planning capabilities with direct optimization algorithms [3-6] to assist the realization of the fluence distributions across beams based on predefined dose distributions. The other requirement is the accessibility to a conventional teletherapy machine including multileaf collimators controlled with specialized computers and software to facilitate the movement of the leaves of the collimator system during the treatment delivery.

The movements of the leaves of the collimator system result in the modulation of intensity across beams to achieve the desired dose distributions within the patient. These requirements are capital intensive and may be costly for a developing country. However, this cost can be minimized by using customized compensating filters fabricated from locally available materials that can account for the effects of the patient's surface irregularities and tissue inhomogeneities [7, 8]. Moreover, the compensating filters can be utilized to address the issues associated with multileaf collimator-based IMRT. These issues include long beam on time [9], complexities of dose verification during treatment delivery [10-12], and dosimetry requirements during commissioning [13].

The use of bolus, wedge filters, or compensators can facilitate the correction of the increase in dose inhomogeneity within an irradiated target volume caused by irregularities in the patient's surface contour [14, 15]. Bolus, which is mostly made from tissue-equivalent materials, is placed on the skin of the patient during the treatment delivery [14, 15]. An unfortunate consequence of using a bolus is the loss of skin sparing associated with megavoltage beams [14, 15].

Howbeit, moving the bolus from the patient surface toward the teletherapy machine radiation source (specifically the block tray position) retains the compensation of the bolus, and also reestablishes the compromised skin sparing [14]. In this case, the bolus can be composed of any non-tissue equivalent material since it is no longer in contact with the patient. This bolus is referred to as a compensating filter (or compensator). The compensating filters are usually placed at the distance of about 15-20 cm from the patient surface [14, 15].

A compensator used to account for a tissue deficit on the patient surface is referred to as a missing tissue compensator [15]. The shape of the compensator must be adjusted based on the position of the compensator relative to the representing bolus to account for beam divergence and reduction in the contributions of scattered photons to dose at any point within the patients [15].

Various approaches have been applied to determine the extent of tissue deficiencies along the surfaces of the patients. Accordingly, various methods have been developed and evaluated to account for the deficiencies with compensating filters [15, 16]. In this regard, wedge filters are used to compensate for missing tissues across sloping surfaces [15]. The application of the wedge filters results in a progressive decrease in the intensity across the beam in certain direction [15].

With this background in mind, the present study aimed to investigate the production of intensity-modulated beams with Aluminium compensating filters in a conventional telecobalt machine based on the outputs of a TPS performing forward planning without direct optimization algorithm, which cannot

directly simulate the presence of a compensating filter in the path of a beam.

The TPS presumes the bolus as part of the patient body; therefore, no additional beam data are required. Bolus is traditionally used in the EBRT to even out the patient skin topography irregularities and increase skin dose [14]. The use of a bolus compromises the skin sparing of megavoltage beams [14].

Theory

The intensity, I, of radiation with initial intensity, I_o, transmitted through an absorber is defined by the Beer-Lambert's equation as [15, 17]:

$$I = I_o e^{-\mu_{eff} x} \quad (1)$$

where μ_{eff} is effective linear attenuation coefficient considering the departure from narrow beam geometry for irradiation geometries in EBRT.

Considering the irradiation geometries for the clinical implementation of a bolus and a compensating filter (Figure 1), the transmitted radiation reaching the detector at a given depth within a phantom, considered to be water for each of the scenarios, is given as the irradiation geometries with the compensating filter and bolus that are determined in the equations (2) and (3), respectively, as follows:

$$\ln\left(\frac{I}{I_0}\right)_c = -\mu_{eff_c} . x_c \quad (2)$$

Where $\left(\frac{I}{I_o}\right)_c$ is the transmission factor for the radiation as it traverses through the compensating filter material, x_c is the thickness of the compensating filter material traversed by the radiation, and μ_{eff_c} is the effective linear attenuation coefficient of the material the compensating filter is made of.

$$\ln\left(\frac{I}{I_0}\right)_b = -\mu_{eff_b} . f . x_b \quad (3)$$

where $\left(\frac{I}{I_o}\right)_b$ is the transmission factor for the radiation as it traverses through the bolus material, x_b is the thickness of bolus material traversed by the radiation, μ_{eff_b} is the effective linear attenuation coefficient of the compensating filter material, and f is a correction factor introduced to account for the effects of the position of the bolus relative to the compensating filter. In this regard, f is the function of field size, thickness of bolus material, source to absorber distance, and depth of measurement within the phantom.

Placing the absorber on the surface of the phantom would increase the transmitted radiation measured at any point within the phantom owing to increase in scattered radiation contribution to dose at any point within the phantom (or patient), compared to the time the absorber is moved away from the surface of the phantom.

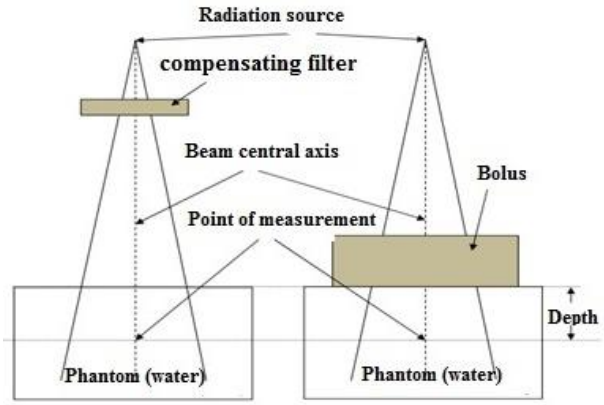

Figure 1. Schematic diagram of irradiation geometry for bolus and compensating filter

To characterize an absorber, it will be very prudent to use the effective mass attenuation coefficient, $\mu_{m_{eff}}$, instead of effective linear attenuation coefficient of the absorber material. This is because Compton effect is the predominant interaction process that occurs when a megavoltage beam for radiotherapy interacts with a material or medium [18]. The Compton effect is dependent on the adsorption coefficient as well as electron and physical densities of the absorber [18]. Therefore, expressing the linear attenuation coefficient of the absorber material in terms of mass attenuation coefficient makes it independent of absorber material density [18]. The effective mass attenuation coefficient of an absorber with density of ρ relates to its effective linear attenuation coefficient as follows:

$$\mu_{m_{eff}} = \frac{\mu_{eff}}{\rho} \quad (4)$$

The substitution of equation (4) into equations (2) and (3) results in equations (5) and (6), respectively:

$$\ln\left(\frac{I}{I_0}\right)_c = -\mu_{m_{effc}} . \rho_c . x_c \quad (5)$$

$$\ln\left(\frac{I}{I_0}\right)_b = -\mu_{m_{effb}} . \rho_b . f . x_b \quad (6)$$

where $\mu_{m_{effc}}$ and $\mu_{m_{effb}}$ are the effective mass attenuation coefficients (in cm^2/g) of the compensating filter and bolus materials, respectively. Additionally, ρ_c and ρ_b are the densities (in g/cm^3) of the compensating filter and bolus materials, respectively.

The compensating filter was used to represent the bolus such that the transmitted radiation at any depth within the phantom would be the same for the two irradiation geometries; therefore, the equations (5) and (6) can be combined to give:

$$\mu_{m_{effc}} . \rho_c . x_c = \mu_{m_{effb}} . \rho_b . f . x_b \quad (7)$$

Rearranging equation (7) gives:

$$x_c = \frac{\mu_{m_{effb}} . \rho_b . f . x_b}{\mu_{m_{effc}} . \rho_c} \quad (8)$$

Since bolus are usually made of tissue-equivalent materials [2, 15], and the densities of those materials can be approximated to that of water (1.0 g/cm^3), equation (8) can be written as:

$$x_c = \left(\frac{k_\mu}{\rho_c}\right) f x_b \quad (9)$$

where k_μ is the ratio of the effective mass attenuation coefficient of bolus material to that of the compensating filter material.

Using equations (1) and (4), it can be shown that the effective mass attenuation coefficient, $\mu_{m_{eff}}$, of an absorber material with density of ρ is given as:

$$\mu_{m_{eff}} = \frac{-\ln\left(I/I_o\right)}{\rho x} \quad (10)$$

where x is the thickness of absorber traversed by the radiation, and $\left(I/I_o\right)$ is the transmission offered by the absorber.

From equation (10), it implies that:

$$k_\mu = \frac{\rho_c x_c}{\rho_b f x_b} \quad (11)$$

Since the density of the bolus material, ρ_b, is similar to that of water. Therefore, equation (11) becomes:

$$k_\mu = \left(\frac{x_c}{f x_b}\right) \rho_c \quad (12)$$

Based on equation (12), it is evident that the direct determination of $\left(\frac{k_\mu}{\rho_c}\right) f$ in equation (9) is to measure the dose with the compensating filter mounted on a tray within a beam irradiated from a teletherapy machine for appropriate field size and depth in a tissue-equivalent phantom. The same measurement was repeated without the compensating filter. In this process, the thickness of the phantom was adjusted to get the same dose as before. The ratio of compensating filter thickness to that of the adjusted thickness of the phantom gives $\left(\frac{k_\mu}{\rho_c}\right) f$. The quantity $\left(\frac{k_\mu}{\rho_c}\right) f$, can therefore be referred to as thickness ratio or density thickness ratio.

Materials and Methods

Prior to performing the experimental measurements, based on the AAPM TG 46 recommendations [19], the quality assurance tests were performed on the teletherapy machine, with beam output of which was to be modulated with the proposed approach. These tests were administered to ensure the accuracy and integrity of the measured beam data, which would be used for the commissioning.

In addition, constancy and stability checks were performed on the ionization chamber, which was used for the beam data acquisitions to ensure the reliability of the measured beam data. These checks were based on the recommendations of the IEC 60731 [20]. The following procedures were used for the effective commissioning of the Aluminium compensating filters for beam intensity modulation based on the proposed approach.

Commissioning

All beam data were measured on the beam central axis with 0.125 cc cylindrical ionization chamber (TW31002-1505, PTW-Freiburg, Germany) in a full scatter motorized water phantom, namely Blue Phantom² (IBA Dosimetry GmbH, Germany). The ionization chamber was connected to a UNIDOS electrometer (10002-20204, PTW-Freiburg, Germany), which was set to measure the output of the teletherapy machine in terms of charges at 60-sec intervals with a chamber bias voltage of +300 V. The teletherapy machine, which was used in this study and whose beam data were acquired, was an Equinox 100 cobalt 60 teletherapy machine (Best Theratronics, Canada).

To measure the thickness ratio for the compensating filter, Aluminium plates with thicknesses of 0-27.45 mm (increments of 3.05 mm) were successively mounted on a block tray and placed in the path of beams irradiated from the telecobalt machine employing isocentric irradiation technique. Each beam had a field size of 10×10 cm². The block tray was placed at the accessories holder on the collimator system of the telecobalt machine.

For each thickness of Aluminium plate mounted on the block tray, the transmitted output of the telecobalt machine was measured with the ionization chamber placed at a depth of 5.0 cm within the phantom and electrometer reading that was corrected for temperature and pressure influences. The above measurements were repeated without the Aluminium plates. The height of water within the phantom was adjusted within 0-20 cm (increments of 2 cm) while keeping the detector at the same depth and maintaining the isocentric irradiation technique.

The electrometer reading was obtained for each adjusted height of water above the detector, and once again corrected for influencing factors (i.e., temperature and pressure). For each thickness of the Aluminium plate, the adjusted height of water above the detector that would give the same corrected electrometer reading as that of a measurement done with a particular thickness of Aluminium plate in the path of the beam was determined. Subsequently, the correlation between the adjusted height of water above the detector and the corresponding thickness of Aluminium that would give the same beam output was calculated.

Additionally, the ratio of Aluminium thickness to the corresponding adjusted height of water above the detector that would give the same beam output was determined for various adjusted heights of water above the detector. A graph of thickness ratio as a function of adjusted height of water above the detector was plotted, and the correlation equation as well as the regression, R^2, of the line of best fit was obtained.

To study the influence of field size (or collimator settings) on the thickness ratio, the above experimental procedures were repeated with a constant thickness of Aluminium plate mounted on the block tray and placed into the path of the beam; however, the field sizes were varied from 3×3 cm^2 to 35×35 cm^2. A constant Aluminium plate thickness of 1.53 cm was used. For each field size setting, the obtained electrometer reading was corrected for influencing factors (i.e., temperature and pressure).

For the measurements involved no Aluminium plate in the path of the beam, the corrected electrometer readings (beam outputs), obtained with the various adjusted heights of water above the detector, were repeated for the various square field sizes. From the aforementioned measurements, we determined the adjusted height of water above the detector for a particular field size that would give the same corrected electrometer reading as that of a measurement with the Aluminium plate in the path of the beam using the same field size.

For each field size, the ratio of the thickness of the applied Aluminium plate placed in the path of the beam during the measurements to the corresponding adjusted height of water above the detector was determined from the measurements involved no compensating filter Nonetheless, the height of water above the detector, adjusted to obtain the same beam output for both measurement scenarios, was calculated for the various field sizes.

The obtained ratios were normalized to that of the reference field size of 10×10 cm^2. The normalized ratios were referred to as field size correction factors. A graph of field size correction factor was plotted against one side of a square field size (equivalent square field size). Furthermore, correlation equation as well as regression, R^2, of the line of best fit were determined.

To study the impact of treatment depth on the thickness ratio, the measurements with varying field sizes were repeated. However, the field size was kept constant at 10×10 cm^2, and the depth of measurement varied within 0.5-17.0 cm. For each depth of measurement with the constant thickness of Aluminium plate in the path of the beam, the output of the telecobalt machine was obtained and corrected for influencing factors (i.e., temperature and pressure).

For the measurements without the Aluminium plate in the path of the beam and with the fixed field size, the electrometer readings (telecobalt machine outputs) obtained for measuring depths ranged within 0.5-32.0 cm. The measured beam outputs (electrometer readings) for the various measuring depths were corrected for variations in air density. From these measurements, for each depth of measurement with the Aluminium plate in the path of the beam, a corresponding depth of measurement without the plate in the path of the beam that would give the same corrected electrometer reading as that with the Aluminium plate in the path of the beam was determined.

The depth of measurement with the Aluminium plate in the path of the beam was subtracted from the determined corresponding depth of measurement without the plate in the path of the beam to determine the related adjusted height of water above the detector. For each depth of measurement, the ratio of the applied Aluminium plate thickness placed in the path of the beam during the measurements to the corresponding adjusted height of water above the detector was obtained from the measurements without the compensating filter.

Nevertheless, the height of water above the detector, adjusted to obtain the same beam output for both measurement scenarios, was calculated for the various depth of measurements. The obtained ratios were normalized to that of the depth of measurement of 5.0 cm with the Aluminium plate in the path of the beam. The normalized ratios were referred to as treatment depth correction factors. A graph of treatment depth correction factor was plotted against the depth of measurement with the Aluminium plate in the path of the beam (treatment depth). Additionally, the correlation equation as well as the regression, R^2, of the line of best fit was calculated.

In all the aforementioned measurements, it was ensured that there was at least 10.0 cm of water below the detector to provide the needed backscattered radiation. The isocentric irradiation technique was also maintained in all the measurements by keeping the position of the detector constant and pumping water into the phantom to obtain the desired depth of measurement. The schematic diagram of the experimental setup is illustrated in Figure 2. To ensure the reproducibility of the experimental outcome, the density and mass attenuation coefficient of the Aluminium were empirically verified.

For the mass attenuation coefficient, the measurements were performed in air for field sizes ranging within 3×3 cm^2 to 30×30 cm^2. The mass attenuation coefficient for each field size was determined as the ratio of measured linear attenuation coefficient for that particular field size to the density of Aluminium. The density of Aluminium was estimated by finding the weights of eight different samples of Aluminium plates used for the study with a digital chemical balance (Mettler Toledo™ ME-TE Precision Balance, Fisher scientific, USA) and dividing the respective weights with their corresponding volumes of Aluminium plates.

The volume of the plate was evaluated based on its physical dimensions measured with an electronic digital caliper (Model # 50003, Chicago Brand Industries, USA). Furthermore, the mean of the determined densities was considered as the density of the Aluminium used in this study.

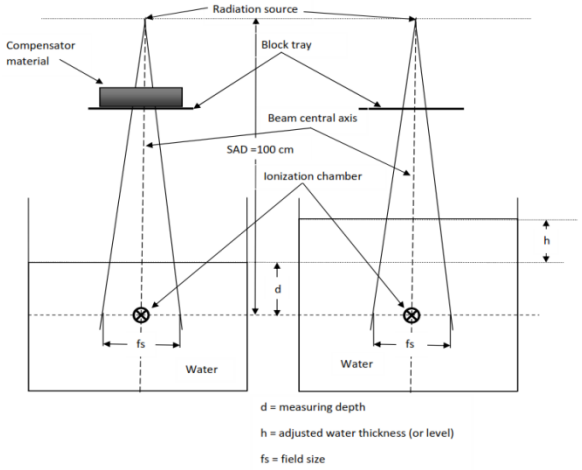

Figure 2. Schematic diagram of experimental setup

Compensating filter construction

In constructing the compensating filter, the length and width were tapered to account for beam divergence. To achieve this aim, a compensating filter sheet with grid lines having grid area of 1×1 cm^2 and two perpendicular lines, running through the central part to represent the major axes of a beam, was designed to record the applied bolus thicknesses along the patient surface. The grid part covered an area of about 2×2 cm^2 at the isocentre of the telecobalt machine.

The thickness of the compensating filter along the direction of beam propagation was also tapered to account for the reduction of scattered radiation contribution to radiation dose at any point within the patient for using the compensating filter as a replacement for bolus during the treatment planning process. After the calculation of the bolus thickness, x_b, within each grid and using equation (9), the thickness, x_c , of a compensating filter along the grid was determined using the following equation:

$$x_c = T_{t_b} f_r f_d x_b \quad (13)$$

Where f_d is the treatment depth correction factor applicable to a specified treatment depth. This value was generally represented by the correlation equation obtained from the plot of depth correction factor against treatment depth for the compensating filter material under consideration. The f_r is the field size correction factor applicable to a particular field size (equivalent square field). This value was represented generally by the correlation equation determined from the plot of field size correction factor against field size for the compensating filter material under consideration. Furthermore, T_{t_b} is the appropriate thickness ratio for a particular thickness of bolus applied within a grid (or along a ray line) under reference conditions (field size of 10×10 cm^2 and treatment depth of 5 cm). This variable was represented by the correlation equation determined from the plot of thickness ratio against the adjusted height of water above the detector.

The thicknesses of the compensating filter at various portions of the radiation field to be modulated were determined and recorded within the respective grids of the compensating filter sheet. Subsequently, the compensating filter sheet with the recorded thicknesses was pasted at the back of transparent Perspex block tray in use for the telecobalt machine. This was performed in such a way that a beam central axis inscribed on the surface of the block tray matched with that of the compensating filter sheet.

The block tray was similar to the one used during the commissioning process. The samples of Aluminium plates used for the commissioning had dimensions of 1×1 cm2 with different thicknesses. These samples were stacked together on the block tray to obtain the stipulated thicknesses of Aluminium within the various grids. The Aluminium plates or blocks were held in place with an adhesive (or bonding agent).

Treatment planning

Treatment simulations were performed with Prowess Panther TPS, version 4.6 (Prowess Inc., USA). A phantom with the dimensions of 30×30×20 cm^3 with radiological properties similar to an acrylic slab phantom (used to verify treatment plans) was created with the TPS using a slice thickness of 5 mm. After the outline of the phantom were delineated on each slice with the auto-contouring tool, multiple plans were generated for the phantom using the plan manager tool. Each plan had a single anterior beam employing source to axis distance treatment technique.

Nevertheless, the field size and treatment depth (i.e., dose prescription depth) for the various plans were different. The plans were named as plan 1, plan 2, plan 3, plan 4, and plan 5. The field sizes of 10×10, 15×6, 25×15, 25×25, and 23×4 cm^2 and treatment depths of 5, 7, 10, 15, and 2 cm were used for plans 1, 2, 3, 4, and 5 to deliver prescribed doses of 100, 150, 200, 250, and 250 cGy at the isocenter, respectively.

During the treatment planning processes with the TPS, beam intensity modulation was achieved by placing the bolus shaped in form of step wedges on the surface of the phantom at the point of beam entrance. It was ensured in each case that the area covered by the bolus extended about 2 cm beyond the radiation field limits (field edges), indicated on the surface of the phantom. Prior to the creation of the bolus, the Hounsfield unit (HU) of the bolus

material was set to that of water (HU=0), which was the default for the TPS.

The axial view of the bolus per case scenario is depicted in the planning windows shown in Figure 3. For each of the plans, the beam central axis was made central to the phantom, and the beam was incident normally to the surface of the phantom. Dose calculation points were then placed at the isocenter along the beam major axis in the direction of the steps of the step wedge. Starting from the beam isocenter, the calculation points were placed at 2 cm apart from each other on either side of the beam central axis as shown in Figure 3A and 3B, respectively.

The step wedges were created such that the middle of the steps were closely in line with the calculation points placed along the beam major axis at the isocenter. Two types of step wedges were created; accordingly, the bolus and the step wedges were referred to as scenarios case 1 and 2, respectively. Various plans were repeated with each type of step wedge of the bolus on the phantom. Dose distributions within the phantom were calculated with various prescribed doses and irradiation geometries in the TPS; furthermore, the corresponding treatment times were recorded for the various plans.

In addition, the off-axis dose profiles along the isocenter in the direction of the step wedge together with their corresponding off-axis distances from the beam central axis were recorded. Bolus thicknesses along the surface of the phantom were determined for the various grids with the aid of available graduated patient origin indicators and measuring tools of the TPS. Subsequently, these measurements were converted to compensating filter thicknesses using equation (13) to facilitate the construction of the compensating filter for each plan.

The various treatment plans, replicated on the telecobalt machine with the replacement of bolus by appropriate Aluminium compensating filters. These filters were constructed based on the developed and proposed approach and placed in the path of the beam. The off-axis doses were measured with calibrated Gafchromic EBT2 film samples (Lot #: 08221302, Ashland Inc., USA). The Gafchromic EBT2 film was calibrated against a 0.6 cc cylindrical ionization chamber (TW 30013, PTW Freiburg, Germany) having traceability to a secondary standard laboratory, based on the International Atomic Energy Agency technical report series 398 protocol [21].

The optical densities of exposed films were read with ImageJ analyzing software (National Institutes of Health, USA). Afterwards, the obtained optical densities were converted to doses using the sensitometric curve of the film determined during the calibration process. The exposed films were scanned with a flatbed scanner (ScanMaker® 9800XL plus, Microtek, USA), and the images were saved in Tagged Image File Format (TIFF) prior to performing the analysis in the ImageJ software. During the dose measurements, the films were sandwiched between the piles of the acrylic slabs forming the phantom (T2967, PTW Freiburg, Germany) at the required treatment depth and held in place by gravity on the treatment couch of the telecobalt machine.

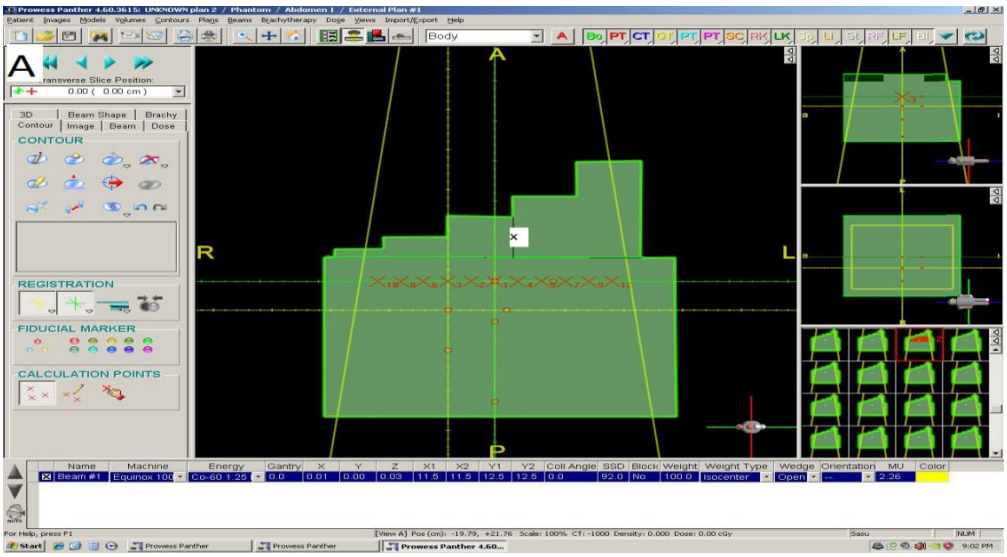

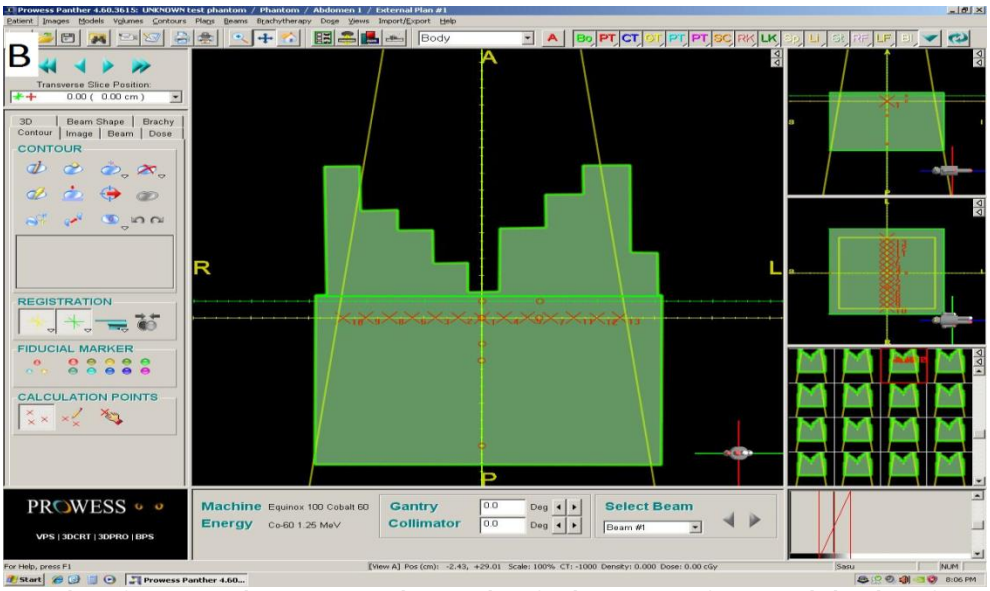

Figure 3. Planning window of treatment planning system showing plans for dosimetry verification, A: bolus shape for case 1, B: bolus shape for case 2

Results

Figure 4 presents the variation of compensating filter (or Aluminium plate) thickness as a function of the adjusted height of water above the detector. The correlation equation as well as the regression, R^2, of the line of best fit is displayed above the curve in Figure 4.

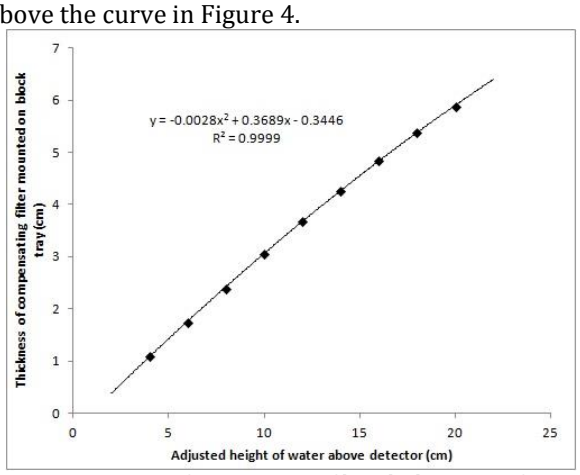

Figure 4. Variation of compensating filter thickness as a function of adjusted height of water above detector

A graph representing the ratio of compensating filter thickness to adjusted height of water above the detector (thickness ratio) against adjusted height of water above the detector is depicted in Figure 5. In addition, the correlation equation and regression, R^2, of the line of best fit are illustrated below the curve in Figure 5.

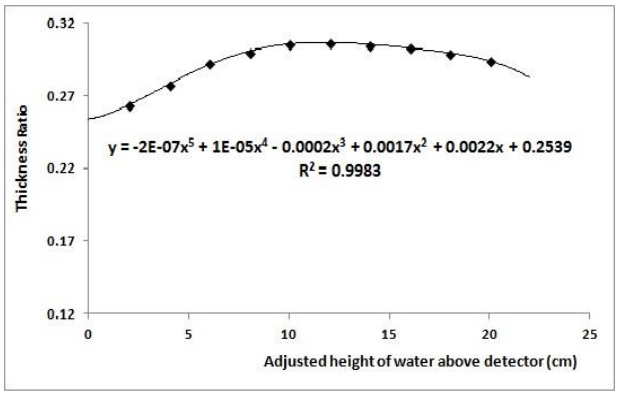

Figure 5. Graph of thickness ratio against adjusted height of water above chamber or simulated bolus thickness

Figure 6 presents a graph of field size correction factor as a function of one side of a square field size. The correlation equation and the regression, R^2, of the line of best fit are depicted above the curve in Figure 6.

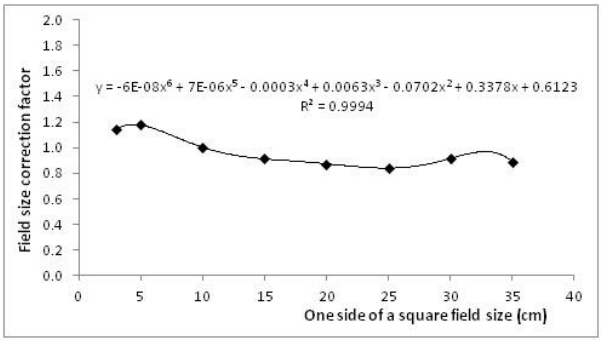

Figure 6. Graph of field size correction factor as a function of field size

A graph illustrating the treatment depth correction factor as a function of the depth of

measurement within the water phantom is demonstrated in Figure 7. Furthermore, above the curve in Figure 7 are displayed the correlation equation and the regression, R^2, of the line of best fit.

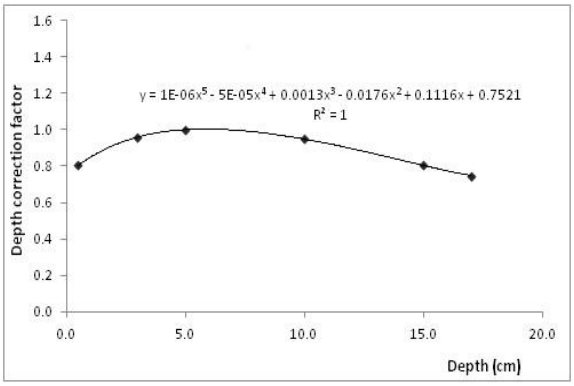

Figure 7. Graph treatment depth correction factor as a function of treatment depth

The variation of mass attenuation coefficient measured in air for the Aluminium used in this study with one side of a square field size is displayed in Figure 8. The correlation equation and the regression, R^2, of the line of best are shown above the curve in Figure 8.

Table 1 presents the measured doses at various calculation points with the Gafchromic films for the compensating filter and the treatment plans replicated on the teletherapy machine for various treatment plans and case scenarios. The calculated doses represent the doses estimated by the TPS with bolus on the surface of the phantom at point of beam entrance. Table 1 also illustrates the deviations between the calculated and the measured doses for

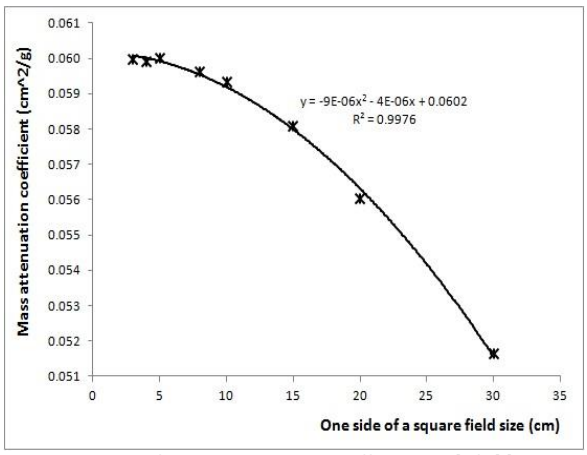

Figure 8. Variation of mass attenuation coefficient with field size

the various calculation points, which are expressed as percentage differences of the respective measured doses.

In this regard, the deviations ranged within -1.3 to 3.98% (mean: 2.55±1.02%) and -4.39 to 4.72% (mean: 3.35±0.94%) for cases 1 and 2, respectively. The omissions in Table 1 indicate places where the calculation points fall outside the steps of the step wedge bolus generated with the TPS.

Based on the graphical manipulations and curve fitting analyses performed on the experimental data, the various terms in equation (13), proposed for converting the applied bolus thickness to Aluminium compensating filter thickness, are given as follows:

$$T_{t_b} = (-2\times10^{-7})t_b{}^5 + (1\times10^{-5})t_b{}^4 - (0.0002)t_b{}^3 + (0.0017)t_b{}^2 + (0.0022)t_b + 0.2539 \quad (14)$$

$$f_r = (-6\times10^{-8})r^6 + (7\times10^{-6})r^5 - (0.0003)r^4 + (0.0063)r^3 - (0.0702)r^2 + (0.3378)r + 0.6123 \quad (15)$$

and

$$f_d = (1\times10^{-6})d^5 - (5\times10^{5})d^4 + (0.0013)d^3 - (0.0176)d^2 + (0.1116)d + 0.7521 \quad (16)$$

where t_b , r and d are applied bolus thickness within a grid of the compensating filter sheet, equivalent square field size and treatment depth, respectively.

Table 1. Comparison of doses for case 1 and case 2

Plan	Calc. Pt	Calculated dose with TPS (cGy)		Measured doses (cGy)		Deviation between doses (%)	
		Case 1	*Case 2*	*Case 1*	*Case 2*	*Case 1*	*Case 2*
1							
	1	100.00	100.00	101.21	101.52	1.20	1.50
	2	98.38	85.08	101.27	88.51	2.85	3.88
	3	92.06	80.29	94.89	83.62	2.98	3.98
	4	86.56	69.38	90.12	72.23	3.95	3.95
	5	82.54	66.79	85.86	69.03	3.87	3.24
2							
	1	150.00	150.00	153.17	153.66	2.07	2.38
	2	148.15	125.75	151.87	130.51	2.45	3.65
	3	146.37	123.47	150.73	128.43	2.89	3.86
	4	129.54	99.70	133.88	103.31	3.24	3.49
	5	126.30	98.48	131.08	103.28	3.65	4.65
	6	159.70	94.90	166.08	98.69	3.84	3.84
	7	121.30	94.80	125.73	99.10	3.52	4.34
3							
	1	200.00	200.00	202.55	200.16	1.26	0.08
	2	198.17	169.79	202.86	175.62	2.31	3.32
	3	196.67	170.48	200.42	175.68	1.87	2.96
	4	175.36	140.83	177.63	144.99	1.28	2.87
	5	174.27	139.99	179.00	145.28	2.64	3.64
	6	220.14	140.00	226.95	144.45	3.00	3.08
	7	173.48	138.45	179.88	144.60	3.56	4.25
	8	214.61	136.12	221.00	141.64	2.89	3.90
	9	167.95	117.51	169.65	120.75	1.00	2.68
	10	206.83	110.05	212.99	114.42	2.89	3.82
	11	208.25	110.82	216.63	115.25	3.87	3.84
	12	130.61	107.56	131.64	109.51	0.78	1.78
	13	123.53	58.01	124.97	55.57	1.15	-4.39
4							
	1	250.00	250.00	254.27	255.57	1.68	2.18
	2	248.60	213.25	255.95	219.33	2.87	2.77
	3	246.85	214.02	252.82	219.42	2.36	2.46
	4	222.63	176.95	227.13	182.67	1.98	3.13
	5	220.48	176.70	228.62	183.18	3.56	3.54
	6	277.75	175.81	288.84	183.02	3.84	3.94
	7	219.26	173.65	224.88	178.10	2.50	2.50
	8	270.00	171.55	281.07	178.59	3.94	3.94
	9	212.27	148.02	217.47	155.32	2.39	4.70
	10	259.69	138.92	263.27	144.56	1.36	3.90
	11	263.04	139.88	266.23	144.50	1.20	3.20
	12	167.20	135.44	168.18	139.03	0.58	2.58
	13	158.14	122.27	162.95	127.30	2.95	3.95
5							
	1	250.00	250.00	254.01	254.01	1.58	1.58
	2	247.82	227.48	255.48	236.17	3.00	3.68
	3	247.62	226.01	254.44	219.68	2.68	-2.88
	4	225.60	195.12	224.59	203.21	-0.45	3.98
	5	224.56	194.58	233.16	204.22	3.69	4.72
	6	266.20	194.76	277.23	202.88	3.98	4.00
	7	221.67	192.11	228.15	199.78	2.84	3.84
	8	261.36	192.08	269.36	197.35	2.97	2.67
	9	185.29	171.04	192.35	179.32	3.67	4.62
	10	251.41	140.66	258.60	144.68	2.78	2.78
	11	-	161.59	-	155.26	-	-4.08
	12	174.62	157.61	172.38	161.42	-1.30	2.36
	13	-	116.81	-	121.49	-	3.85

Calc. Pt: measured doses at various calculation points, TPS: treatment planning system

Discussion

The Aluminium used in this study had a measured density of 2.70±0.03 g/cm^3. Furthermore, for the field sizes ranged from 3×3 cm^2 to 30×30 cm^2, ~~and~~ the in air mass attenuation coefficients were found to range within 0.05163-0.06000 cm^2/g (mean: 0.058074±0.002937 cm^2/g). The value of mass attenuation coefficient generally decreased with increasing field size due to the enhancement of scattered radiation contribution to dose at the beam central axis along with field size.

The scattered radiation comes from the jaws of the collimator system and the radiation source encapsulation itself. As field size increases, the surface area of a particular jaw exposed to the radiation elevates, which results in the production of more scattered radiation. The correlation between the mass attenuation coefficient and field size can be expressed with a second degree polynomial. The measured density and the value of the mean mass attenuation coefficient of Aluminium for various field sizes compared favourably well with those stated in the literature [22].

The aforementioned radiological properties (i.e., density and mass attenuation coefficient) affect radiation scattering and absorption characteristics of the compensating filter material. Therefore, these properties would have influence on the proposed equation for converting an applied bolus thickness to a compensating filter thickness. The constants within the various polynomial equations expressing the correction factors would be dependent on the radiological properties.

Consequently, it is necessary to verify and validate the density and mass attenuation coefficient of the material chosen for the construction of the compensating filter prior to the implementation of the proposed approach. It can also be inferred that the various correction factors introduced would be dependent on beam energy (quality). Since the correction factors are related to scattered radiation, anything that affects the scattering would influence the correction factors. As a result, the correction factors would be dependent on the collimator system design of a teletherapy machine.

The measurements with the adjusted heights of water above the detector were used to simulate or mimic the bolus in the path of beams. Since bolus is composed of tissue-equivalent materials, it was very convenient to use water to represent the bolus. Moreover, representing the bolus with water made it very easy to change the thickness of the bolus during the measurements.

The correlation equations (or coefficients) of the curves, depicted in figures 5, 6 and 7, were used to express and determine the thickness ratio needed to convert the bolus thickness to compensating filter thickness for any applied bolus thickness, obtain the appropriate correction factor to be incorporated for any field size, and specify the proper correction factor for any treatment depth, respectively.

Furthermore, the respective regression values were closely approaching or equal to unity for the lines of best fits as shown in figures 5, 6 and 7. This signifies that these correlation equations can be used to predict with great accuracy the thickness ratio, field size correction factor, and treatment depth correction factor based on their respective correlated treatment parameters.

The depth of measurement within the water phantom is synonymous to treatment depth with regards to a patient. Using the expression for a correlation equation would facilitate the determination of a required factor from any related treatment parameter, and also help in generalizing the proposed equation. To simplify the computational process for converting a bolus thickness to compensating filter thickness, lookup tables may be generated for the required factors. However, in the present study, Microsoft spreadsheet (Microsoft Inc., USA) was applied for performing various calculations.

The measurements with and without the compensating filter demonstrated that the introduced correction factors for the stipulated treatment parameters could be expressed as fifth degree polynomial equations in terms of treatment depth and applied bolus thickness, respectively, and a sixth degree polynomial in terms of field size by using the graphical considerations and curve fitting analyses of the empirical data.

The high degree of the polynomial equations necessitates to be cautious about not using treatment parameters beyond the limits applied for the empirical determination of the correction factors and thickness ratio. Accordingly, lack of attention to this issue will constitute uncertainties in a determined dose within the patient. Consequently, it is prudent to include all ranges of bolus thickness, field size, and treatment depths as likely to be used for clinical applications during the commissioning process.

For the field size correction factor, a correlation was established for square field sizes. Field size correction factors may be determined for other non-square field sizes through the concept of equivalent square field size [23-37]. The one side of a square field size used for the plot corresponds to an equivalent square field size. Therefore, the determination of the equivalent square field size for a particular non-square field size and substitution of this value into the correlation equation gives the required field size correction factor that needs to be applied to account for the influence of field size on the thickness ratio.

All the measurements were performed with isocentric (source to axis distance) irradiation

technique since it is the therapeutic method of choice that is frequently used in the radiotherapy department where the study is being conducted. The majority of the doses that were measured during the replication of treatment plans on the telecobalt machine were higher than those calculated with the TPS. This shows that the proposed approach generally undercompensates the beam output. This could be attributed to the challenges encountered with the fabrication of the compensating filter to obtain the required thickness, which resulted from the method used in constructing the filter. Regarding this, other methods may be used for the construction of the compensating filter once the shape of the filter is determined based on the proposed approach.

In the present study, similar approach was used with a constant thickness ratio for a particular beam energy. Furthermore, the effects of field size, bolus/compensating thickness, and treatment depth were ignored, which resulted in encouraging results (measured doses after transmitting through the compensator showed discrepancies within ±5% from what was expected) for missing tissue compensation [15]. The application of the proposed approach led to dose discrepancies of ± 4.73% from what was expected. This value is within the recommended dose tolerance of ±5% required for dose delivery in EBRT [38].

Ignoring the inherent uncertainties associated with film dosimetry [39, 40] supports the assertion that apart from the separation between the patient surface and compensating filter, other treatment parameters have marginal influence on the required thickness ratio for a particular beam energy [15, 41]. Nonetheless, the dose verification procedure needs to be repeated with other two-dimensional array detectors based on ionization chamber or diode.

In other studies investigating compensating filters, some of the researchers incorporated the effects of off-axis distance in their respective approaches for the determination of the compensating filter thickness. This was due to the fact that most of their beam data were acquired on the beam central axis and compensation needed to be done at other parts of the radiation field other than on the beam central axis [42, 43]. It is also expected that if the effects of the off-axis distance are also considered in the proposed approach, there will be much improvement in the output of the proposed approach.

Nevertheless, there were some challenges with the proposed approach. In this regard, the determination of the applied bolus thicknesses for beams with oblique incidence relative to the surface of the phantom were quiet challenging and cumbersome. Moreover, there was limitation with the thickness of the bolus that could be applied since it should not have been more than 14 cm. This issue made it impossible to simulate situations requiring high levels of compensation, which are frequently encountered in IMRT.

In addition, the use of abutting fields were problematic when there was overlap of fields since the TPS did not allow for entering bolus for individual radiation field. The constant thickness of Aluminium plate used in the measurements to assess the field size and treatment depth correction factors was chosen such that there were always significant scattered radiation in the forward direction and low noise to signal ratios. This was done to facilitate the variation of field size or treatment depth whilst keeping the other treatment parameters constant. Nevertheless, there is ongoing research to assess the influence of varying the constant thickness of the Aluminium plate used in the determination of the field size and treatment depth correction factors.

Conclusion

In the present study, we outlined the procedures of determining the shape of a compensating filter made of Aluminium and constructing the compensating filter for a conventional telecobalt machine to produce a desired dose distribution within a patient based on the output of a TPS performing forward planning, which cannot directly simulate the compensating filter. The outputs of the proposed approach compared favorably well to those of the TPS based on the dose verification measurements performed with samples of calibrated films in a solid water phantom for various irradiation geometries.

The discrepancies in the measured doses, compared to those of the TPS, were within ±4.73% (mean of 2.98±1.05%). This signifies that the proposed approach can be recommended for clinical application. Therefore, the use of the proposed approach could facilitate the generation of intensity-modulated beam with limited resources using the missing tissue approach rendering encouraging results.

The proposed approach might be suitable for beam intensity modulations where the possibility of realizing the beam intensity map is not available. This approach can be used for missing tissue compensation in the treatment of head and neck cancers, tangential breast irradiation, and total body irradiation with photon beams. It can also be used to account for tissue heterogeneities, especially in the treatment of lung cancers. Generally, the proposed approach can be used to enhance the conformity index of dose coverage in EBRT.

Acknowledgement

The completion of this study could not have been possible without the involvement and assistance of co-workers at the National Centre for Radiotherapy,

Korle Bu Teaching Hospital, Accra, Ghana, whose names may not all be enumerated. Their contributions are sincerely appreciated and gratefully acknowledged. However, I would like to express my deep appreciation and indebtedness particularly to Professor A. W. K. Kyere and C. Schandorf, Dr. Joel Yarney and S. Y. Opoku, and my PhD advisory team assigned by the University of Cape Coast, Ghana, for their endless support as well as kind and understanding spirit during the research period.

I would also like to express my gratitude to the manager of the Sweden Ghana Medical Centre, Accra, Ghana, for letting me have access to their three-dimensional motorized water phantom (Blue Phantom^2) for the beam data acquisition.

Another thanks goes to all relatives, friends, and others who in one way or another shared their support morally, financially, or physically.

Above all, my appreciation and thanks to the Great Almighty, the author of knowledge and wisdom, for his countless love.

References

1. Schlegel W, Bortfeld T, Grosu A. New technologies in radiation oncology. Springer-Verlag Berlin Heidelberg, Germany. 2006.
2. Podgorsak E. B. Radiation oncology Physics: A handbook for teachers and students. International Atomic Energy Agency (IAEA). 2005.
3. Brewster L, Mohan R, Mageras G, Burman, C, Leibel S, Fuks Z. Three dimensional conformal treatment planning with multileaf collimators. Int. J. Rad. Onc. Biol. Phys. 1995 Dec 1; 33(5): 1081–9. DOI: 10.1016/0360-3016(95)02061-6.
4. McNair HA, Adams EJ, Clark CH, Miles EA, Nutting CM. Implementation of IMRT in the radiotherapy department. Br J Radiol. 2003 Dec;76(912): 850-6. DOI: 10.1259/bjr/19737738.
5. Vaarkamp J, Adams EJ, Warrington AP, Dearnaley DP. A comparison of forward and inverse planned conformal, multi segment and intensity modulated radiotherapy for the treatment of prostate and pelvic nodes. Radiother. Oncol. 2004 Oct; 73(1):65-72. DOI: 10.1016/j.radonc.2004.07.015.
6. Shepard DM, Earl M A, Li X A, Naqvi S, Yu C. Direct aperture optimization: A turnkey solution for step-and-shoot IMRT. Med. Phys. 2002 Jun; 29 (6): 1007-18. DOI: 10.1118/1.1477415.
7. Chang S. Compensating filter-intensity-modulated Radiotherapy – A Traditional Tool for Modern Application. Radiotherapy and Imaging. 2006: 82- 6.
8. Vassy D L, Turmel J, Josey J C. Solid Modulation: Problem-Solving IMRT. American College of Radiology. 2008 Nov; 5(11): 1150 - 3. DOI: 10.1016/j.jacr.2008.08.001.
9. Rawlinson JA, Islam MK, Galbraith DM. Dose to radiation therapists from activation at high-energy accelerators used for conventional and intensity-modulated radiation therapy. Med Phys. 2002 Apr; 29(4): 598–608. DOI: 10.1118/1.1463063.
10. George R, Keall PJ, Kini VR, et al. Quantifying the effect of intrafraction motion during breast IMRT planning and dose delivery. Med Phys 2003; 30: 552–62. DOI: 10.1118/1.1543151.
11. Buckey CR, Stathakis S, Papanikolaou N. The inter- and intrafraction reproducibilities of three common IMRT delivery techniques. Med. Phys. 2010; 37(9): 4854 - 60. DOI: 10.1118/1.3476413.
12. Chang SX, Cullip TJ, Deschesne KM. Intensity modulation delivery techniques: "Step & shoot" MLC auto sequence versus the use of a modulator. Med Phys. 2000 May; 27(5): 948–59. DOI: 10.1118/1.598989.
13. Sharma SD. Challenges of small photon field dosimetry are still challenging. Journal of medical physics/Association of Medical Physicists of India. 2014 Jul;39(3):131-2. DOI: 10.4103/0971-6203.138998. .
14. Stanton R, Stinson D. Applied physics for radiation oncology. Revised edition. Medical Physics Publishing. 2009.
15. Khan FM. The Physics of Radiation Therapy. Fourth Edition. Lippincott Williams and Wilkins. 2010.
16. O-Hoon C, Jung-Eun L, Hong-Seok N, Doo-Kwon B. Modeling for Missing Tissue Compensator Fabrication Using RFID Tag in U-Health . International Symposium on Biological and Medical Data Analysis. Biological and Medical Analysis. 2006: 463-71.
17. Paliwal BR, Rommelfanger S, Das RK. Attenuation characteristics of a new compensating filter material: Thermo-Shield for high energy electron and photon beams. Med. Phys. 1998 Apr; 25(4): 484 - 7. DOI: 10.1118/1.598223.
18. Report of Task Group No. 65 of the Radiation Therapy Committee of the American Association of Physicists in Medicine: AAPM Report 85. Tissue inhomogeneity corrections for megavoltage photon beams. American Association of Physicists in Medicine. 2004 Jul: 3- 107.
19. Kutcher G J, Coia L, Gillin M, Hanson W F. et al. Comprehensive QA for radiation oncology: Report of AAPM radiation therapy committee task group 40. Med. Phys. 1994 Apr; 21(4): 581- 618. DOI: 10.1118/1.597316.
20. International Electrotechnical Commission (IEC): Medical electrical equipment – Dosimeters with ionization chambers as used in radiotherapy. IEC 60731. IEC. 1997.
21. International Atomic Energy Agency (IAEA). Technical report series 398. Absorbed dose determination in external beam radiotherapy. IAEA. 2000.
22. National Institute of Standards and Technology (NIST),USA. Physical measurement laboratory. *Available from:* http://physics.nist.gov.
23. Day, M.J., A note on the calculation of dose in x-ray fields. British Journal of Radiology. 1950; 23(270): 368-9.
24. Day MJ, Aird EG. The equivalent field method for dose determinations in rectangular fields. Br J Radiol Suppl. 1983;17:105-14.
25. Bjärngard BE, Siddon RL. A note on equivalent circles, squares, and rectangles. Medical physics. 1982 Mar 1;9(2):258-60. DOI: 10.1118/1.595161.

26. Clarkson, J.R. A note on depth doses in fields of irregular shape. British Journal of Radiology. 1941 Aug; 14(164): 265- 8. DOI: 10.1259/0007-1285-14-164-265.
27. Sathiyan S, Ravikumar M, Keshava SL. Relative Output Factors and Absolute Equivalent Square Fields at Depths for High Energy X-Ray and Gamma Ray Beams. Austral Asian Journal of Cancer. 2006; 5(4): 225-35.
28. Sterling T, Perry H, and Weinkam J. Automation of radiation treatment planning. VI. A general field equation to calculate percent depth dose in the irradiated volume of a cobalt 60 beam. Br. J. Radiol. 1967 Jun; 40(474): 463-74. DOI: 10.1259/0007-1285-40-474-463.
29. Vadash P, Bjärngard B. An equivalent-square formula for head scatter factors. Med Phys. 1993 ; 20(3):733-4. DOI: 10.1118/1.597024.
30. Monti AF, Ostinelli A, Frigerio M, Gelosa S. An equivalent square method for irregular photon fields. Med Dosim. 1995 Winter; 20(4): 275-7.
31. Sanz, DE. Accuracy limits of the equivalent field method for irregular photon fields. Phys Med Biol. 2002 Sep 7; 47(17): 3073-85.
32. Thomas SJ, Eaton DJ, Tudor GS, Twyman NI. Equivalent squares for small field dosimetry. Br J Radiol. 2008 Nov; 81(971): 897-901. DOI: 10.1259/bjr/27713136.
33. Araki F, Ikeda R, Moribe N, Shirakawa Y, Hatemura M, Shi-monobou T, et al. Dose calculation for asymmetric photon fields with independent jaws and multileaf collimators. Med Phys. 2000 Feb; 27(2): 340-5. DOI: 10.1118/1.598836.
34. Kwa W, Kornelsen RO, Harrison RW, el-Khatib E. Dosimetry for asymmetric x-ray fields. Med Phys. 1994 Oct; 21(10):1599-604. DOI: 10.1118/1.597260.
35. Day MJ. The equivalent field method for axial dose determinations in rectangular fields. Br J Radiol. 1972;11: 95-10.
36. Tagoe SNA, Nani EK, Yarney J, et al. Semi-empirical equivalent field method for dose determination in midline block fields for cobalt-60 beam. Journal of Applied Science and Technology. 2012; 17: 70 - 7.
37. Chengeni N, Tahmasebi Birgani MJ. Equivalent field calculation for irregular symmetric and asymmetric photon fields. International Scholarly and Scientic research and innovation. 2013; 7(9): 1430 - 5.
38. International Atomic Energy Agency (IAEA). IAEA-TECDOC-896. Radiation dose in radiotherapy from prescription to delivery. IAEA, Vienna. 1996.
39. Martišíková M, Ackermann B, Jäkel O. Analysis of uncertainties in Gafchromic® EBT film dosimetry of photon beams. Phys. Med. Biol. 2008 Nov 18;53(24):7013. DOI: 10.1088/0031-9155/53/24/001.
40. Devic S, Seuntjens J, Hegyi G, , Podgorsak EB, et al. Dosimetric properties of improved GafChromic films for seven different digitizers. Med. Phys. 2004 Sep 1; 31 (9): 2392 - 401. DOI: 10.1118/1.1776691.
41. Levitt SH, Purdy JA, Perez CH, Vijayakuma S. Technical basis of radiation therapy: Practical clinical application. 4th Revised Edition. Springer; 2008.
42. Haghparast A, Hashemi B, and Eivazi M T. Influence of compensator thickness, field size, and off-axis distance on the effective attenuation coefficient of a cerrobend compensator for intensity-modulated radiation therapy. Medical Dosimetry. 2013 Spring; 38(1): 25-9. DOI: 10.1016/j.meddos.2012.06.001.
43. Iwasaki A, KuIwasaki A, Kubota M, Fujimori A, Suzaki K, Abe Y, et al. Formulation of spectra-based attenuation coefficients in water as a function of depth and off-axis distance for 4, 10 and 15MV X-ray beams. Radiation Physics and Chemistry. 2005 Apr; 72(6): 657-61. DOI: 10.1016/j.radphyschem.2004.05.051.